



ISSN: 0095-8972 (Print) 1029-0389 (Online) Journal homepage: <http://www.tandfonline.com/loi/gcoo20>


Coordination of di- and triimine ligands at ruthenium(II) and ruthenium(III) centers: structural, electrochemical and radical scavenging studies

Irvin N. Booyesen, Abimbola Adebisi, Matthew P. Akerman, Orde Q. Munro & Bheki Xulu


To cite this article: Irvin N. Booyesen, Abimbola Adebisi, Matthew P. Akerman, Orde Q. Munro & Bheki Xulu (2016) Coordination of di- and triimine ligands at ruthenium(II) and ruthenium(III) centers: structural, electrochemical and radical scavenging studies, *Journal of Coordination Chemistry*, 69:10, 1641-1652, DOI: [10.1080/00958972.2016.1177177](https://doi.org/10.1080/00958972.2016.1177177)

To link to this article: <http://dx.doi.org/10.1080/00958972.2016.1177177>

 View supplementary material 

 Accepted author version posted online: 11 Apr 2016.
Published online: 06 May 2016.

 Submit your article to this journal 

 Article views: 111

 View related articles 

 View Crossmark data 

 Citing articles: 1 View citing articles 

Coordination of di- and triimine ligands at ruthenium(II) and ruthenium(III) centers: structural, electrochemical and radical scavenging studies

Irvin N. Booyesen, Abimbola Adebisi, Matthew P. Akerman, Orde Q. Munro and Bheki Xulu

School of Chemistry and Physics, University of KwaZulu-Natal, Pietermaritzburg, South Africa

ABSTRACT

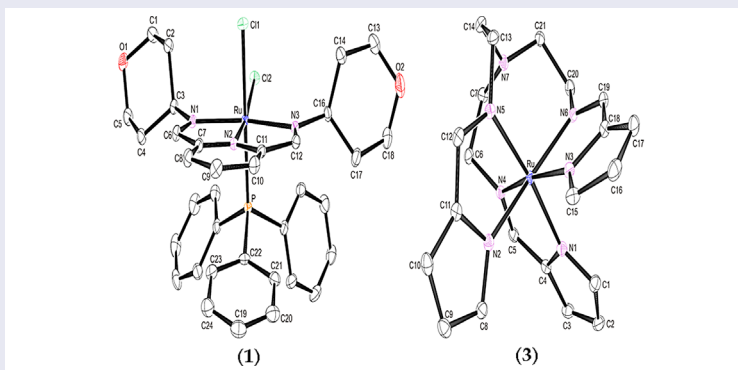
Herein, we explore the coordination of di- and triimine chelators at ruthenium(II) and ruthenium(III) centers. The reactions of 2,6-bis-((4-tetrahydropyrimidinomethyl)pyridine) (thppy), N^1, N^2 -bis((3-chromone)methylene)benzene-1,2-diamine (chb), and *tris*-((1*H*-pyrrol-2-ylmethylene)ethane)amine (H_3 pym) with *trans*-[Ru^{II}Cl₂(PPh₃)₂] afforded the diamagnetic ruthenium(II) complex *cis*-[RuCl₂(thppy)(PPh₃)] (**1**) and the paramagnetic complexes [*mer*-Ru₂(μ-chb)Cl₆(PPh₃)₂] (**2**), and [Ru(pym)] (**3**), respectively. The complexes were characterized by IR, NMR, and UV-vis spectroscopy and molar conductivity measurements. The structures were confirmed by single crystal X-ray diffraction studies. The redox properties of the metal complexes were probed via cyclic- and squarewave voltammetry. Finally, the radical scavenging capabilities of the metal complexes towards the NO and 2,2-di(4-*tert*-octylphenyl)-1-picrylhydrazyl (DPPH) radicals were investigated

ARTICLE HISTORY

Received 10 July 2015
Accepted 10 February 2016

KEYWORDS


Ruthenium; imine; crystal structure; redox properties; radical scavenging activity



1. Introduction

The discovery of NAMI-A, *trans*-[Ru^{III}Cl₄(DMSO)(Im)](ImH) (ImH = protonated imidazole) as a potential ruthenium metallopharmaceutical has led to a resurgence of interest in the coordination chemistry of ruthenium in medicinal inorganic chemistry [1–4]. Ligands utilizing chelators with neutral nitrogen

CONTACT Irvin N. Booyesen ✉ Booyesen@ukzn.ac.za

 Supplemental data for this article can be accessed at <http://dx.doi.org/10.1080/00958972.2016.1177177>.

donors (e.g. $[\text{Ru}(\text{bpy})_3]^{2+}$) have proven advantageous with respect to the stabilization of ruthenium in both high and low oxidation states [4–6]. In addition, the high metal-binding affinity of this class of ligands makes them excellent candidates as bifunctional chelators of ruthenium centers and as scaffolds incorporating biologically relevant moieties [7, 8]. The inclusion of biologically relevant ligands in coordination complexes of ruthenium is geared towards improving cell specificity of the metal complexes, thereby potentially minimizing side effects with respect to healthy cells [9, 10].

Our research is closely aligned with this design strategy for discovering new ruthenium metallo-pharmaceuticals. More specifically, we have explored the coordination of Schiff bases derived from biologically relevant moieties towards ruthenium(II) and (III) centers [11–14]. The reactions of *trans*- $[\text{RuCl}_2(\text{PPh}_3)_3]$ with the diimine ligands 2,6-*bis*-((6-amino-1,3-dimethyluracilimino)methylene)pyridine (H_4ucp) and 2,6-*bis*-((antipyrene-imino)methylene)pyridine (bpap) readily afforded $[\text{Ru}^{\text{II}}(\text{H}_3\text{ucp})\text{Cl}(\text{PPh}_3)]$ and *cis*- $[\text{Ru}^{\text{II}}\text{Cl}_2(\text{bpap})(\text{PPh}_3)_2]$, respectively [11]. The dinuclear ruthenium complex, $[\text{Ru}_2^{\text{III}}(\mu\text{-Cl})_2\text{Cl}_2(\text{Hchpr})_2(\text{PPh}_3)_2]$ (H_2chpr = 2-amino-3-((tetrahydro-2*H*-pyran-4-ylimino)methyl)-4*H*-chromen-4-one), exhibits optimal redox properties governed by the well-defined Ru(II/III) and Ru(III/IV) redox couples observed within its cyclic voltammogram. The redox properties induced significantly higher DPPH radical scavenging activity than the corresponding free ligand, H_2chpr and the natural antioxidant, vitamin C [13].

In this study, we have investigated the coordination modes of di- and triimines towards ruthenium(II) and ruthenium(III). More specifically, the diamagnetic ruthenium(II) complex, *cis*- $[\text{RuCl}_2(\text{thppy})(\text{PPh}_3)]$ (**1**), and the paramagnetic ruthenium(III) complexes [*mer*- $\text{Ru}_2(\mu\text{-chb})\text{Cl}_6(\text{PPh}_3)_2$] (**2**) and $[\text{Ru}(\text{pym})]$ (**3**) were isolated from the 1 : 1 M reactions of *trans*- $[\text{Ru}^{\text{II}}\text{Cl}_2(\text{PPh}_3)_3]$ with 2,6-*bis*-((tetrahydropyranimino)methyl)pyridine (thppy), *N*¹,*N*²-*bis*-((chromone)methylene)benzene-1,2-diamine (chb) or *tris*-((1*H*-pyrrol-2-yl-methylene)ethane)amine (H_3pym), respectively. To evaluate the antioxidant potential of the ruthenium complexes, radical scavenging studies were conducted with DPPH and NO radicals. Notably, the biologically significant components of the present complexes (*viz.* pyrrole, chromone, and tetrahydropyran) and their derivatives are known to exhibit both antioxidant and anticancer activities [13, 15, 16]; hence the inclusion of these moieties in metal complexes could potentially promote target-specific delivery to malignant tumors.

2. Experimental

2.1. Materials and methods

Trans- $[\text{RuCl}_2(\text{PPh}_3)_3]$, 2,6-dicarboxaldehyde-pyridine, tetrahydro-2*H*-pyran-4-amine, 1,2-diaminobenzene, 3-formylchromone, pyrrole-2-carboxaldehyde, *tris*-(2-aminoethyl)amine, 2,2-di(4-*tert*-octylphenyl)-1-picrylhydrazyl (DPPH), Griess reagent, sodium nitroprusside, phosphate buffered saline tablets, and electrochemical analysis grade tetrabutylammonium hexafluorophosphate were obtained from Sigma Aldrich. All solvents and common salts were obtained from Merck SA. Reagent grade toluene was dried over sodium wire, while the chemicals and other solvents were used without purification. Ultrapure water was produced from an Elga Purelab Ultra system. The synthetic procedures and characterization data for the free ligands (*viz.* thppy, chb, H_3pym) can be found in the online supporting information document, see figures S1–S6.

Infrared spectra were recorded on a Perkin-Elmer Spectrum 100 from 4000 to 350 cm^{-1} . The ^1H and ^{31}P NMR spectra were obtained using a Bruker Avance 400 MHz spectrometer. All NMR spectra were recorded in $\text{DMSO}-d_6$. UV–vis spectra were recorded using a Perkin Elmer Lambda 25. The extinction coefficients (ϵ) are given in $\text{M}^{-1} \text{cm}^{-1}$. The X-band electron paramagnetic resonance (EPR) spectra of **2** and **3** were obtained at 298 K from a Bruker EMX Ultra X-band spectrometer. Melting points were determined using a Stuart SMP3 melting point apparatus. Conductivity measurements were determined at 295 K on a Radiometer R21M127 CDM 230 conductivity and pH meter.

Voltammetric measurements were done using an Autolab potentiostat equipped with a three electrode system: a glassy carbon working electrode (GCWE), a pseudo $\text{Ag}|\text{AgCl}$ reference electrode and

an auxiliary Pt counter electrode. The Autolab Nova 1.7 software was utilized for the operation of the potentiostat and data analysis. The ruthenium complexes were made up of 2 mM solutions in CH_2Cl_2 (for **1** and **2**) and $\text{DMSO}:\text{CH}_3\text{CN}$ (1 : 1, $v:v$ for **3**) along with tetrabutylammonium hexafluorophosphate (0.1 M) as a supporting electrolyte. Between each measurement, the GCWE electrode surface was polished with a slurry of ultrapure water and alumina on a Buehler felt pad followed by rinsing with excess ultrapure water and ultra-sonication in absolute ethanol.

The experimental procedures of the radical scavenging studies were adapted from literature methods [17, 18]. All experiments were run in triplicate and the percentage radical scavenging activities were determined via the following equation:

$$\% \text{Radical scavenging activity} = [(A_c - A_f)/A_c] \times 100$$

where A_c is the absorbance of the control (DPPH or NO radicals) and A_f is the absorbance upon addition of the ligand or metal complex to the control. In turn, the IC_{50} values of the respective ligands and their metal complexes were calculated from the individual percentage radical scavenging activities. First, the UV-vis spectrum of the control (0.2 mM solution of DPPH in DCM) was measured and thereafter a 0.1 cm^3 of the metal complex or the free ligand [$30 \mu\text{M}$ in DCM (for **1**, **2** and ligands) and $\text{DMSO}:\text{CH}_3\text{CN}$ (for **3**)] were added. The resultant solutions were shaken vigorously, left to stand for 20 min in the dark and thereafter their respective UV-vis spectra were measured.

The NO radical assay was done using the following experimental procedure: a 5 mM solution of sodium nitroprusside was prepared in a phosphate buffered saline solution. After an incubation period of 3 h, the Griess reagent (0.5 cm^3) was added to 0.3 cm^3 of the nitroprusside solution. The UV-vis spectrum of this mixture was taken (which constitutes the "control"). The sample solutions were prepared by adding 0.3 cm^3 of sodium nitroprusside solution to 1 cm^3 of the metal complex or the free ligand ($30 \mu\text{M}$ in DMSO) and allowing the resultant mixtures to incubate for 3 h at room temperature. After the incubation period, 0.5 cm^3 of the Griess reagent was added which was followed by analysis through UV-vis spectroscopic measurements.

2.2. *cis*-[RuCl₂(thppy)(PPh₃)] (1)

A 1 : 1 M reaction mixture of thppy (0.0314 g, 104 μmol) and *trans*-[RuCl₂(PPh₃)₂] (0.100 g, 104 μmol) was heated under reflux in toluene (20 cm^3) for 6 h. From the resulting dark purple solution, a maroon precipitate was attained. This precipitate was dissolved in dichloromethane and layered with hexane. XRD quality dark crystals were obtained from the layered solution after several days. M.p. > 350 °C, yield = 80% (based on Ru). IR ($\nu_{\text{max}} \text{ cm}^{-1}$): $\nu(\text{C}=\text{N})$ 1635 (w), $\nu(\text{O}-\text{C}-\text{O})_{\text{thp}}$ 1134, 1081 (vs), $\nu(\text{Ru}-\text{PPh}_3)$ 698, $\nu(\text{Ru}-\text{N})$ 525. ¹H NMR (295 K ppm⁻¹): 8.28 (s, 2H, H6, H12), 7.70–7.12 (m, 18H, H8, H9, H10, PPh₃), 4.34 (t, 2H, H5, H18), 3.95–3.86 (m, 2H, H5', H18'), 3.80–3.71 (m, 2H, H1, H13); 3.15 (t, 2H, H1', H13'); 2.72 (t, 2H, H4, H17); 2.40–2.19 (m, 2H, H44', H17'); 1.99–1.74 (m, 2H, H2, H14); 1.31–1.21 (m, 2H, H2', H14'); 0.61 (d, 2H, H3, H16). ³¹P NMR (295 K ppm⁻¹): 30.58. Conductivity (DCM, 10⁻³ M): 12.5 $\Omega \text{ cm}^2 \text{ mol}^{-1}$. UV-vis (DCM, λ_{max} (ϵ , M⁻¹ cm⁻¹)): 239 nm (52,195); 297 nm (sh, 6644); 317 nm (sh, 5137); 332 nm (sh, 3356); 461 nm (5848); 571 nm (2522); 688 nm (sh, 469).

2.3. [mer-Ru₂(μ -chb)Cl₆(PPh₃)₂] (2)

A mixture of chb (0.0276 g, 104 μmol) and *trans*-[RuCl₂(PPh₃)₂] (0.100 g, 104 μmol) in toluene (20 cm^3) and one drop of 32% hydrochloric acid was heated under reflux for 6 h. A dark brown precipitate was filtered and washed with toluene as well as diethyl ether. Upon addition of 10 cm^3 acetonitrile to the filtrate, the slow evaporation of the resultant mixture afforded brown crystals suitable for X-ray analysis. M.p. > 350 °C, yield = 77% (based on Ru). IR ($\nu_{\text{max}} \text{ cm}^{-1}$): $\nu(\text{N}-\text{H})$ 2950, 2938, 2846 (m), $\nu(\text{C}=\text{N})_{\text{imine}}$ 1615 (s), $\nu(\text{O}-\text{C}-\text{O})$ 1159, 1143 (m), $\nu(\text{Ru}-\text{PPh}_3)$ 692 (vs), $\nu(\text{Ru}-\text{N})$ 526 (vs), $\nu(\text{Ru}-\text{O})$ 455 (w). Conductivity (DCM,

10^{-3} M): 12.66 Ω cm² mol⁻¹. UV-vis (DCM, λ_{max} (ϵ , M⁻¹ cm⁻¹): 263 nm (sh, 19,164); 360 nm (13,173); 454 nm (sh, 8522); 723 nm (sh, 1465).

2.4. [Ru(pym)] (3)

Equimolar quantities of H₃pym (0.0394 g, 104 μ mol) and *trans*-[RuCl₂(PPh₃)₃] (0.100 g, 0.104 mmol) were heated at reflux temperature for 8 h in toluene (20 cm³). A dark precipitate was filtered and washed with toluene, MeOH, CH₃CN, DCM, and diethyl ether. Slow evaporation of the filtrate gave dark brown crystals. M.p. >350 °C, yield = 91% (based on Ru). IR (ν_{max} cm⁻¹): $\nu(\text{C}=\text{N})_{\text{imine}}$ 1605 (sh, s), $\nu(\text{C}=\text{N})_{\text{heterocyclic}}$ 1573 (vs), $\nu(\text{Ru}-\text{N})$ 524, 513 (vs). Conductivity (DMSO/CH₃CN (1:1, ν : ν), 10^{-3} M): 16.95 Ω cm² mol⁻¹. UV-vis (DMSO/CH₃CN, λ_{max} (ϵ , M⁻¹ cm⁻¹): 291 nm (17,531); 361 nm (sh, 10,891).

2.5. X-ray diffraction

The X-ray data for the metal complexes were recorded on a Bruker Apex Duo equipped with an Oxford Instruments Cryojet operating at 100(2) K and an Incoatec microsource operating at 30 W power. Crystal and structure refinement data are given in table 1. Selected bond lengths and angles are given in tables 2–4 for **1**·H₂O, **2**·CH₃CN, and **3**, respectively. In all three cases, the data were collected with Mo K α (λ = 0.71073 Å) radiation at a crystal-to-detector distance of 50 mm. The following conditions were used for data collection: omega and phi scans with exposures taken at 30 W X-ray power and 0.50° frame widths using APEX2 [19]. The data were reduced with SAINT [19] using outlier rejection, scan speed scaling, as well as standard Lorentz and polarization correction factors. A SADABS semi-empirical multi-scan absorption correction [20] was applied to the data. Direct methods, SHELXS [21], and WinGX [22] were used to solve all three structures. All non-hydrogen atoms were located in the difference density map and refined anisotropically with SHELXL-2014 [21]. All hydrogens were included as idealized contributors in the least squares process. Their positions were calculated using a standard riding model with C–H_{aromatic} distances of 0.93 Å and $U_{\text{iso}} = 1.2 U_{\text{eq}}$, C–H_{methylene} distances of 0.99 Å and $U_{\text{iso}} = 1.2 U_{\text{eq}}$ and C–H_{methyl} distances of 0.98 Å and $U_{\text{iso}} = 1.5 U_{\text{eq}}$. The O–H bonds of water molecule for **1** were located in the difference density map and refined isotropically.

Table 1. Crystal data and structure refinement data.

	1·H ₂ O	2·CH ₃ CN	3
Chemical formula	C ₃₅ H ₄₀ Cl ₂ N ₃ O ₃ PRu	C ₆₆ H ₅₂ Cl ₆ N ₄ O ₄ P ₂ Ru ₂	C ₂₁ H ₂₄ N ₂ Ru
Formula weight	753.64	1441.92	475.54
Temperature (K)	100(2)	100(2)	100(2)
Crystal system	Monoclinic	Orthorhombic	Cubic
Space group	<i>P</i> 2 ₁ / <i>n</i>	<i>P</i> 2 ₁ 2 ₁ 2	<i>I</i> -43 <i>d</i>
Unit cell dimensions (Å, °)	<i>a</i> = 15.1098(5) <i>b</i> = 13.5262(5) <i>c</i> = 16.6804(6) α = 90 β = 97.080(2) γ = 90	<i>a</i> = 16.168(1) <i>b</i> = 20.6678(13) <i>c</i> = 9.2012(6) α = 90 β = 90 γ = 90	<i>a</i> = 19.9699(7) <i>b</i> = 19.9699(7) <i>c</i> = 19.9699(7) α = 90 β = 90 γ = 90
<i>V</i> (Å ³)	3383.1(2)	3074.6(3)	7963.9(8)
<i>Z</i>	4	2	16
Density (Calcd) (Mg m ⁻³)	1.480	1.577	1.586
Absorption coefficient (mm ⁻¹)	0.708	0.857	0.810
<i>F</i> (0 0 0)	1522	1456	3888
θ range for data collection (°)	1.7; 27.1	1.60; 26.00	2.50; 30.01
Reflections measured	22,561	11,872	13,549
Observed reflections [<i>I</i> > 2 σ (<i>I</i>)]	6565	5479	1804
Independent reflections	7443	5863	1913
Data/restraints/parameters	7443/2/414	5863/1/384	1913/0/88
Goodness of fit on <i>F</i> ²	1.022	1.091	1.061
Observed <i>R</i> , <i>wR</i> ²	0.025; 0.060	0.031; 0.076	0.024; 0.0487
<i>R</i> _{int}	0.026	0.022	0.043

Table 2. Selected bond lengths (Å) and angles (°) for **1**.

N1–Ru–N2	78.71(6)
N2–Ru–N3	78.73(6)
N2–Ru–Cl2	170.09(4)
N1–Ru–N3	157.42(6)
C6–N1–C3	121.2(1)
C12–N3–C16	118.5(1)
Ru–N1	2.061(2)
Ru–N3	2.090(2)
Ru–P1	2.3099(5)
Ru–Cl1	2.4324(5)
Ru–Cl2	2.4707(5)

Table 3. Selected bond lengths (Å) and angles (°) for **2**.

O1–Ru1–N1	89.5(1)
Cl2–Ru1–Cl3	167.60(5)
Ru1–N1	2.159(4)
Ru1–P1	2.330(1)
Ru1–Cl1	2.324(1)
Ru1–Cl2	2.332(1)
Ru1–Cl3	2.355(1)
Ru1–O1	2.083(3)
C8–O1	1.251(5)
C6–O2	1.333(7)
C5–O2	1.373(6)

Table 4. Selected bond lengths (Å) and angles (°) for **3**.

^a N _{pyrrole} –Ru–N _{imino}	77.94(8)
N _{imino} –Ru–N _{imino}	100.32(9)
N _{pyrrole} –Ru–N _{imino}	172.37(9)
Ru–N _{imino}	2.070(2)
Ru–N _{pyrrole}	2.049(2)

^aBite angles.

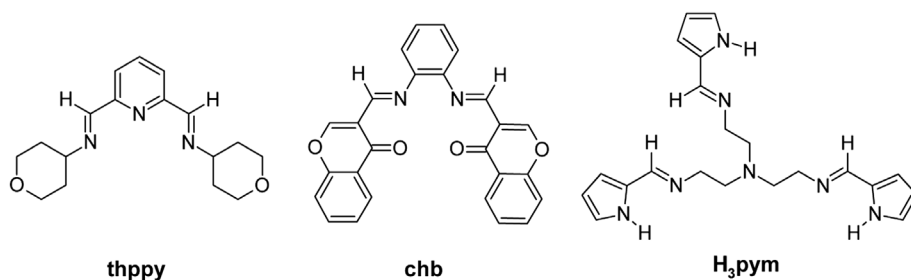
3. Results and discussion

3.1. Synthesis and spectral characterization

The isolated ruthenium complexes **1**–**3** were synthesized from equimolar reactions of trans-[RuCl₂(PPh₃)₃] with the respective Schiff bases: thppy, chb, or H3pym. In **1**, the thppy moiety is a neutral tridentate chelator through its (NN)iminoNpy donor set while for chb moiety bridges two mer-[RuIIICl₃] cores via its ketonic oxygen and imino nitrogens. In the synthesis of dinuclear **2**, initially the hydrochloric acid oxidizes the metal centers by H⁺, leading to hydrogen gas evolution from the reaction mixture [23, 24]. Coordination of chloride anions and the chelator to the metal centers resulted in **2** being formed. In **3**, the triimine pym chelator substituted all the ligands of the metal precursor, coordinating to ruthenium through its three imino nitrogens and three deprotonated pyrrolidine nitrogens. In fact, this phenomenon has been observed in coordination of trans-[RuCl₂(PPh₃)₃] with analogous tripodal triimine ligands derived from tris-(2-aminoethyl)amine [25]. However, the rigid ruthenium(II) arene cores remained intact for the organometallic ruthenium(II) complexes, [Ru(Ar)Cl(sal3tr)] (sal3tr = tris-2-(salicylaldimine ethyl)amine) and [Ru(Ar)Cl(py3tr)] (py3tr = tris-2-(2-pyridylimine ethyl)amine) where the arene (Ar) core can be hexamethylbenzene, para-cymene, or hydroxyethoxybenzene [26].

Complexes **1** and **2** are highly soluble in high boiling point aprotic and chlorinated solvents, while **3** is only partially soluble in a 1 : 1 (v : v) mixture of DMSO and acetonitrile. The low molar conductivity values of the formulated metal complexes affirm that they are non-electrolytes [11, 27]. Only low resolution EPR spectra could be obtained for **2** and **3** which are typical of ruthenium(III) complexes with distorted octahedral geometries [28, 29], figure S7. In the ¹H NMR spectrum of **1** the imino protons

appear as a sharp singlet (at 8.28 ppm), which are shifted downfield from the analogous hydrogens in the free ligand, thppy, at 7.98 ppm (see figure S8). In the 7.07–7.12 ppm aromatic region, a multiplet integrates to 18 protons ascribed to the pyridyl moiety and the triphenylphosphine ligand. The uncoordinated tetrahydropyran (thp) moieties are characterized by the expected upfield multiplet signals in the NMR spectrum between 3 and 4 ppm. Both thp moieties exhibit chair conformations in solution as evidenced by the lack of signals from boat conformers of the six-membered rings (this is consistent with the X-ray data for **1**, *vide infra*). As expected, only one signal is observed in the ^{31}P NMR spectrum of **1** from the triphenylphosphine ligand.



The IR spectra of the free ligands contain strong vibrations that are readily assigned to the imine C=N groups at 1643 cm^{-1} (for thppy), 1635 cm^{-1} (for chb), and 1644 cm^{-1} (for H₃pym), see figures S4–S6. Noticeably, these vibrations are at significantly lower frequencies in the IR spectra of the respective metal complexes, *viz.* 1635 cm^{-1} for **1**, 1615 cm^{-1} for **2**, and 1605 cm^{-1} for **3**, consistent with metal-to-ligand back-donation into π^* molecular orbitals involving the C=N groups, which partly reduces the C=N bond order and thus stretching frequency of the C=N group relative to the free ligand. The intense stretching modes of the Ru–P bonds, $\nu(\text{Ru}-\text{PPh}_3)$, for **1** and **2** are at 698 and 692 cm^{-1} , respectively. In **1**, the C–O–C ether group stretches of the uncoordinated thp moieties occur at identical frequencies to those of the free ligand, thppy [$\nu(\text{O}-\text{C}-\text{O}) = 1081$ and 1134 cm^{-1}]. This reflects no interaction between the thp groups and ruthenium. For **2**, the broad C–O–C ether group vibration (1131 cm^{-1}) of free chb appears as a medium-intensity split vibration (at 1159 and 1143 cm^{-1}) in the IR spectrum of the metal complex. The absence of the pyrrole N–H vibrations in the IR spectrum of **3** reflects deprotonation of the pyrrole rings and their coordination to ruthenium(III). Ru–N vibrational modes of the metal complexes are comparable with one another, while the Ru–O vibrational mode appears at 455 cm^{-1} .

The UV–vis spectral analysis reveals that several common intraligand $\pi-\pi^*$ electronic transitions are shared among the free ligands and their respective metal complexes, see figures S9–S11. Furthermore, metal-to-ligand charge transfer (MLCT) bands at 461 and 571 nm for **1** are observed and despite its d^6 low-spin electron configuration, a metal-based (at 688 nm) electronic transition with a low extinction coefficient is observed. However, for the paramagnetic ruthenium(III) complexes, only a weak d–d transition for **2** is observed at 723 nm . The absence of the metal-based electronic transition of **3** is ascribed to a higher band-gap energy, whereas in **1**, a narrow band-gap energy makes the d–d electronic transition favorable [30].

3.2. Voltammetry analysis

Initially, the cyclic voltammetry of **3** was conducted in a 1 : 1 (*v* : *v*) solvent mixture of DMSO and CH_3CN since this complex is insoluble in DCM. Noteworthy for **3**, the use of coordinative solvents can potentially influence the redox behavior of **3** as solvents such as DMF and DMSO typically induce axial coordination of metallophthalocyanines which in turn results in metal-based redox processes [31]. The cyclic voltammograms (CVs) of **1** and **2** in DCM show one and two redox processes, respectively (see figures 1 and S12). All redox couples are quasi-reversible as their peak-to-peak separations (ΔE) are different [$\Delta E(\mathbf{1}) = 150\text{ mV}$, $\Delta E(\mathbf{2-A}) = 81\text{ mV}$ and $\Delta E(\mathbf{2-B}) = 80\text{ mV}$] than that of the ferrocene standard [$\Delta E(\text{ferrocene-DCM}) = 90\text{ mV}$ versus $\text{Ag}|\text{AgCl}$] under the same experimental conditions. The redox

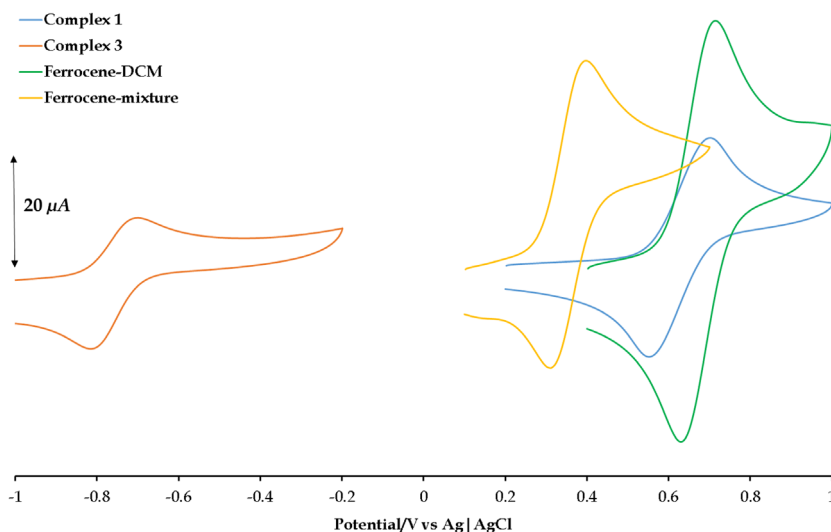


Figure 1. Cyclic voltammograms (CVs) of **1** and **3** as well as their corresponding ferrocene standards at a scan rate of 100 mV s^{-1} conducted in DCM (*viz.* ferrocene-DCM) and the DMSO:CH₃CN mixture (*viz.* ferrocene-mixture).

processes exhibit diffusion-controlled behavior at increasing scan rates and have peak current ratios approaching 1. This suggests that each redox process corresponds to a one electron redox process. The single quasi-reversible redox couples observed in the CVs of **1** and **3** [$\Delta E(\mathbf{3}) = 110 \text{ mV}$ against the $\Delta E(\text{ferrocene-mixture}) = 100 \text{ mV}$] are consistent with the Ru(II/III) redox process as the halfwave potentials [$E_{1/2}(\mathbf{1}) = 0.625 \text{ V}$ and $E_{1/2}(\mathbf{3}) = -0.755 \text{ V}$ versus Ag|AgCl] compare favorably with other ruthenium(II) and (III) complexes where the voltammetric studies have been conducted in either coordinating or non-coordinating solvents [11, 30, 32]. Complex **2** mimics the redox behavior of dinuclear $[\text{Ru}_2^{\text{III}}(\mu\text{-Cl})_2\text{Cl}_2(\text{Hchpr})_2(\text{PPh}_3)_2]$ ($\text{H}_2\text{chpr} = 2\text{-amino-3-}((\text{tetrahydro-2H-pyran-4-ylimino)methyl)\text{-4H-chromen-4-one}$) with the Ru(II/III) [$E_{1/2} = -0.143 \text{ V}$ versus Ag|AgCl] and Ru(III/IV) [$E_{1/2} = 0.158 \text{ V}$ versus Ag|AgCl] redox couples denoted as **A** and **B** in figure S12 [13].

3.3. Radical scavenging studies

Abnormally high concentrations of free radicals in the human body are associated with oxidative and nitrosative stress which can potentially lead to cancer, Alzheimer's disease, and cardiovascular disease [33–35]. The radical scavenging properties of ruthenium complexes can be compared with the natural antioxidant vitamin C and organic-based synthetic radical scavengers (e.g. butylated hydroxytoluene). The attractive attribute of these metal-based compounds is readily accessible oxidation states of ruthenium which makes them effective scavengers of free radicals. More specifically, the radical scavenging capabilities of ruthenium complexes can be enhanced either by donation of an electron or a hydrogen from an organic ligand of the ruthenium complexes [36–38]. Furthermore, as the biologically significant components (*viz.* thp in **1**, chromone in **2** and pyrrole in **3**) are known antioxidants, the presence of the latter ligands can potentially enhance the radical scavenging capabilities of **1–3**.

The influence of the redox active metal center is clearly observed with an increase in the radical scavenging activity of the metal complexes in comparison to the free ligand. Most notable is the NO radical scavenging activity of **2** [$\text{IC}_{50}(\text{NO}) = 143 \mu\text{M}$] versus thppy [$\text{IC}_{50}(\text{NO}) = 308 \mu\text{M}$], refer to table 5. The metal complexes have lower IC_{50} values than the natural antioxidant, vitamin C [$\text{IC}_{50}(\text{NO}) = 210 \mu\text{M}$ and $\text{IC}_{50}(\text{DPPH}) = 147 \mu\text{M}$], with the exception of **1** (for NO) and **3** (for DPPH) [17, 18]. As mentioned earlier, the dinuclear complex, $[\text{Ru}_2^{\text{III}}(\mu\text{-Cl})_2\text{Cl}_2(\text{Hchpr})_2(\text{PPh}_3)_2]$, exhibits similar redox behavior to **2**. This is also reflected in their similar DPPH scavenging capabilities [13]. In addition, the chromone-derived Schiff

Table 5. IC₅₀ values (in μM) of the ruthenium compounds and free ligands. Each IC₅₀ value has a standard deviation less than 8% with respect to its mean value.

	NO	DPPH
1	231	44
2	143	87
3	151	194
thppy	527	54
chb	199	118
H ₃ pym	308	289

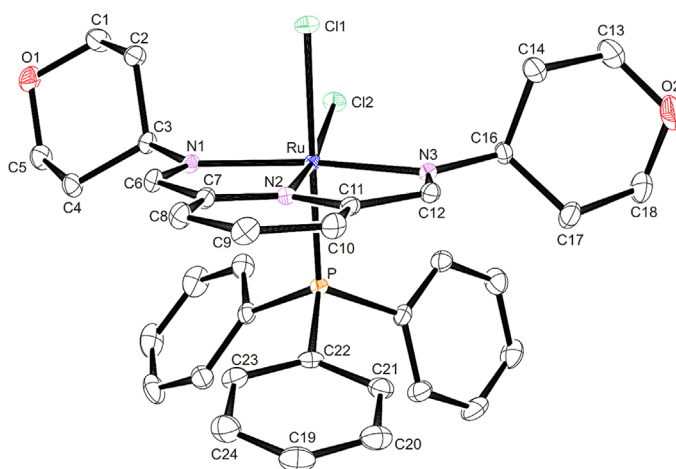
base neutralizes the NO and DPPH radicals more effectively compared to vitamin C while the thp free ligand has comparable DPPH radical scavenging abilities with vitamin C.

3.4. Crystal structures of 1–3

3.4.1. Crystal structure of 1

Complex **1** co-crystallizes with a water molecule of crystallization in the space group $P2_1/n$ (figure 2). Each monoclinic unit cell contains four molecules of **1**·H₂O and the crystal lattice is stabilized by a network of hydrogen bonding occurring between **1**·H₂O dimers in which the water molecules bridge the complexes by hydrogen bonds involving the coordinated chlorides (see figure S13). Within each dimer, these hydrogen bonding interactions induce the formation of an intermolecular four-membered ring [Cl2···H1S–O3/Cl2A···H1SA–O3A = 2.25(3) and Cl2A···H2S–O3/Cl2···H2SA–O3A = 2.30(3) Å]. Furthermore, an intramolecular ring···ring π -type interaction occurs between the nearly co-planar pyridyl moiety and the C19–C24 phenyl ring of the PPh₃ co-ligand (centroid···centroid distance, 3.511(1) Å, plane-to-plane angle, 18.73(6) Å; see figure S14).

Surprisingly in **1**, the Ru–N_{imino} bond distances [Ru–N1 = 2.061(2) and Ru–N3 = 2.090(2) Å] are not equidistant; this is accompanied by commensurate differences for the opposing C=N–C bond angles [C6–N1–C3 = 121.2(1)° and C12–N3–C16 = 118.5(1)°]. The anomalies in the above geometrical parameters probably reflect minor differences in the positions of the thp moieties in three-dimensional space. The coordination sphere octahedron of **1** is distorted as evidenced by the non-perpendicular bite angles [N1–Ru–N2 = 78.71(6)° and N2–Ru–N3 = 78.73(6)° for **1**]. This deviation from octahedral coordination is emphasized further by deviation from linearity of the equatorial bond angles for **1** [N2–Ru–Cl2 = 170.09(4)° and N1–Ru–N3 = 157.42(6)°]. Furthermore, the variable *trans*-influences of the N2 and

**Figure 2.** An ORTEP view of **1** showing 50% probability displacement ellipsoids and the atom labeling. The hydrogens and water of crystallization were omitted for clarity.

P atoms effective on the chloro co-ligands accounts for the differences in the Ru–Cl bond distances of **1** [Ru–Cl1 = 2.4324(5) and Ru–Cl2 = 2.4707(5) Å].

3.4.2. Crystal structure of **2**

The asymmetric unit of **2** comprises a single ruthenium ion coordinated by three chlorides and a triphenylphosphine ligand (figure 3). The fifth and sixth coordination sites of the octahedron are occupied by the chromone carbonyl and imine nitrogen of the Schiff base ligand. The potentially tetradentate ligand acts as two bidentate ligands bridging two metal centers. The other half of the dinuclear species is related to the asymmetric unit by crystallographically imposed two-fold rotation symmetry which bisects the phenyl ring ($Z = 2$).

The crystal lattice of **2** is made up of concentric columns of **2** which run parallel both to the $[a]$ - and $[b]$ -axes. This arrangement of the molecules is conferred via intermolecular interactions between approximately co-planar phenyl rings of PPh_3 and the annealed phenyl rings of the chromone (plane-to-plane angle, $6.4(2)^\circ$) with a ring centroid...centroid distance of 3.798(3) Å (see figure S15). An example is the interaction of the C14'–C19' phenyl ring of the P(1') Ph_3 of **2** with respect to the C1–C5C9 ring of a chromone moiety of an adjacent molecule and the interaction between the C14 and C19 phenyl ring of the triphenylphosphine co-ligand and the C1'–C5'C9' ring of the chromone moiety of a neighboring molecule.

Although the bridging phenyl moiety (of the chb chelator in **2**) lies out of the planes of the chromone by 88.20° and these moieties also form a dihedral angle of 65.31° , the geometrical parameters around

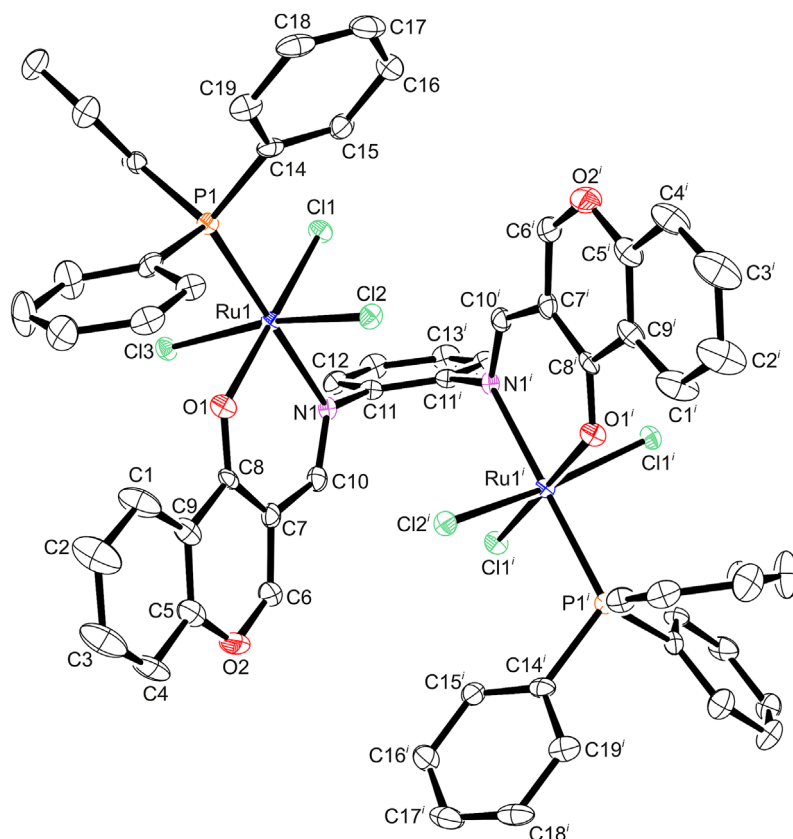


Figure 3. An ORTEP view of **2** showing 50% probability displacement ellipsoids and the atom labeling. The hydrogens and ethanol of crystallization were omitted for clarity. Symmetry code: (i) $-x, -y, z$.

each ruthenium in **2** are identical. Indicative to **1**, the constrained O1–Ru1–N1 [89.5(1)°] bite angle of **2** induces deviation in its axial bond angle [Cl2–Ru1–Cl3 = 167.60(5)°]. The Ru–N_{imino} bond lengths are considerably shorter in the paramagnetic **2** [Ru–N_{imino} = 2.159(4) Å] due to high Lewis acid character of Ru(III) compared to the diamagnetic character of **1**. As expected, the same trend is found when comparing the Ru–P [2.3099(5) Å for **1** and 2.330(1) Å for **2**] and Ru–Cl [Ru1–Cl1 = 2.324(1), Ru1–Cl2 = 2.332(1) and Ru1–Cl3 = 2.355(1) Å for **2**] coordination sphere bonds. These meridionally arranged chloro co-ligands in **2** have comparable bond lengths to other compounds containing the *mer*-[RuCl₃]³⁺ core [39–41].

The bond orders of the carbonyl-like C8–O1/C8ⁱ–O1ⁱ double bonds of **2** are clearly established based on their shorter bond distances [1.251(5) Å] in comparison with the ether-type C–O bonds [O2–C6/O2ⁱ–C6ⁱ = 1.333(7) and O2–C5/O2ⁱ–C5ⁱ = 1.373(6) Å]; in effect, these bonds are in their ketonic forms. The Ru–O_{ketonic} bond distance [2.083(3) Å] differs clearly from the literature-based Ru^{III}–O_{phenolate} bond distances in *trans*-[Ru(L)Cl(PPh₃)₂] [1.9906(15) Å] (H₂L = 2-hydroxy-1-naphthaldehyde-benzoylhydrazine), [Ru(pyhz)₂]ClO₄ [1.971(2) Å] (Hpyhz = 2-((2-(pyridin-2-yl)hydrazono)methyl)phenol), and [Ru(pzpo)(acac)] (H₂pzpo = 1,2-*bis*(2-(1-methyl-1*H*-pyrazol-3-yl)phenol)benzene) [1.983(3) and 2.008(3) Å] [42–44].

3.4.3. Crystal structure of **3**

Compound **3** exhibits an octahedral geometry with all six coordination sites occupied by the hexadentate Schiff base ligand (figure 4). The asymmetric unit is composed of a single ruthenium ion with a site occupancy of a third. This metal ion is coordinated by a deprotonated pyrrole ring and imine nitrogen. The imine group is appended to the central bridging amine. Application of the crystallographically imposed three-fold rotation axis which runs through the central amine and ruthenium generates the octahedral complex (*Z* = 16).

In comparison to **1**·H₂O and **2**·CH₃CN, the larger unit cell dimensions of **3** allow 16 molecules of **3** to pack in its cubic unit cell. This complex displays a significantly distorted octahedral geometry imposed on by its five- [N_{pyrrole}–Ru–N_{imino} = 77.94(8)°] and eight-membered [N_{imino}–Ru–N_{imino} = 100.32(9)°] chelate rings. Also in **3**, due to the presence of the non-delocalized bridging aliphatic amine, its Ru–N_{imino} bond distances of 2.070(2) Å are shorter than those of **2**. In addition, the identical Ru–N_{pyrrole} [2.049(2) Å] bond lengths of **3** were in the range [2.037(6)–2.082(9) Å] found for other ruthenium to monoanionic pyrrole nitrogen bonds [45–48].

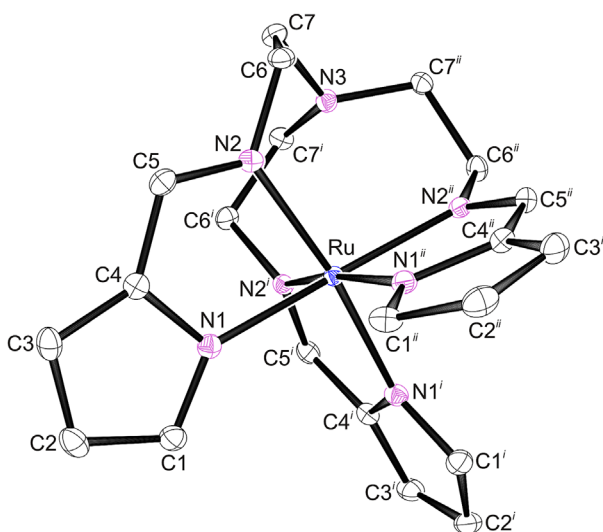


Figure 4. An ORTEP view of **3** showing 50% probability displacement ellipsoids and the atom labeling. The hydrogens were omitted for clarity. Symmetry codes: (i) $-\frac{1}{2} + x, \frac{1}{2} - y, 1 - z$; (ii) $1 - x, \frac{1}{2} + y, \frac{1}{2} - z$.

4. Conclusion

Exploring the coordination of the diimines (*viz.* thppy and chb) and the triimine (*viz.* H₃pym) to the *trans*-[Ru(PPh₃)₂]²⁺ core afforded complexes with diverse structural features: *cis*-[RuCl₂(thppy)(PPh₃)] (**1**), [*mer*-Ru₂(μ-chb)Cl₆(PPh₃)₂] (**2**), and [Ru(pym)] (**3**). The thppy chelator of **1** is a neutral tridentate ligand through its (NN)_{imino}N_{py} donor set, while the neutral chb ligand of **2** bridges the two *mer*-[Ru^{III}Cl₃] cores via its ketonic oxygen and imino nitrogen. The triimine ligand pym displaces all ligands of the ruthenium precursor affording the six-coordinate *tris*(pyrrolide-imine) chelate of Ru(III), **3**. All the metal complexes have lower IC₅₀ values compared with their corresponding free ligands. The complexes were also more effective scavengers compared with the naturally occurring antioxidant vitamin C.

Supplementary material

CCDC 1407274-1407276 contains crystallographic data for this article. These data can be obtained free of charge at www.ccdc.cam.ac.uk/conts/retrieving.html [or from the Cambridge Crystallographic Data Center (CCDC), 12 Union Road, Cambridge CB2 1EZ, UK; Fax: +44(0)1223-336033; E-mail: deposit@ccdc.cam.ac.uk]. Supplementary figures S1–S15 associated with this article can be found in the online version.

Acknowledgements

We are grateful to the University of KwaZulu-Natal and the National Research Foundation of South Africa for financial support.

Disclosure statement

No potential conflict of interest was reported by the authors.

Funding

This work was financially supported by the South African Agency for Science and Technology Advancement, National Research Foundation of South Africa and University of KwaZulu-Natal.

References

- [1] D. Gambino, L. Otero. *Inorg. Chim. Acta*, **393**, 103 (2012).
- [2] A.K. Singh, D.S. Pandey, Q. Xua, P. Braunstein. *Coord. Chem. Rev.*, **270–271**, 31 (2014).
- [3] A. Bergamo, C. Gaiddon, J.H.M. Schellens, J.H. Beijnen, G. Sava. *J. Inorg. Biochem.*, **106**, 90 (2012).
- [4] F. Li, J.G. Collins, F.R. Keene. *Chem. Soc. Rev.*, **44**, 2529 (2015).
- [5] T. Rawling, A. McDonagh. *Coord. Chem. Rev.*, **251**, 1128 (2007).
- [6] Q. Sun, S. Mosquera-Vazquez, Y. Suffren, J. Hankache, N. Amstutz, L.M.L. Lawson Daku, E. Vauthey, A. Hauser. *Coord. Chem. Rev.*, **282–283**, 87 (2015).
- [7] K. Ypsilantis, S. Karkabounas, E. Georgiou, I. Zelovitis, A. Garoufis. *Inorg. Chim. Acta*, **421**, 152 (2014).
- [8] S.M. Cloonan, R.B.P. Elmes, M.L. Erby, S.A. Bright, F.E. Poynton, D.E. Nolan, S.J. Quinn, T. Gunnlaugsson, D.C. Williams. *J. Med. Chem.*, **58**, 4494 (2015).
- [9] D. Sun, Y. Liu, Q. Yu, D. Liu, Y. Zhou, J. Liu. *J. Inorg. Biochem.*, **150**, 90 (2015).
- [10] S. Wanninger, V. Lorenz, A. Subhan, F.T. Edelmann. *Chem. Soc. Rev.*, **44**, 4986 (2015).
- [11] I.N. Booyesen, S. Maikoo, M.P. Akerman, B. Xulu. *Polyhedron*, **79**, 250 (2014).
- [12] I.N. Booyesen, A. Adebisi, O.Q. Munro, B. Xulu. *Polyhedron*, **73**, 1 (2014).
- [13] I.N. Booyesen, A. Adebisi, M.P. Akerman. *Inorg. Chim. Acta*, **433**, 13 (2015).
- [14] I.N. Booyesen, S. Maikoo, M.P. Piers Akerman, B. Xulu, O. Munro. *J. Coord. Chem.*, **66**, 3673 (2013).
- [15] N. Phosrithong, J. Ungwitayatorn. *Bioorg. Chem.*, **49**, 9 (2013).
- [16] M.N. Narule, M.K. Gaidhane, P.K. Gaidhane. *J. Pharm. Res.*, **6**, 626 (2013).
- [17] P. Krishnamoorthy, P. Sathyadevi, K. Senthilkumar, P. Thomas Muthiah, R. Ramesh, N. Dharmaraj. *Inorg. Chem. Commun.*, **14**, 1318 (2011).
- [18] R. Ramachandran, P. Viswanathamurthi. *Spectrochim. Acta, Part A*, **103**, 53 (2013).
- [19] Bruker APEX2, SAINT and SADABS, Bruker AXS Inc., Madison, Wisconsin, USA (2010).

- [20] R.H. Blessing. *Acta Cryst.*, **A51**, 33 (1995).
- [21] G.M. Sheldrick. *Acta Cryst.*, **C71**, 3 (2015).
- [22] L.J. Farrugia. *J. Appl. Cryst.*, **45**, 849 (2012).
- [23] C. Tan, J. Liu, H. Li, W. Zheng, S. Shi, L. Chen, L. Ji. *J. Inorg. Biochem.*, **102**, 347 (2008).
- [24] M.B. Cingi, M. Lanfranchi, M.A. Pellinghelli, M. Tegoni. *Eur. J. Inorg. Chem.*, **2000**, 703 (2000).
- [25] S. Mandal, D.K. Seth, P. Gupta. *Polyhedron*, **31**, 167 (2012).
- [26] B.C.E. Makhubela, M. Meyer, G.S. Smith. *J. Organomet. Chem.*, **772–773**, 229 (2014).
- [27] N.G. Tsierekzos, A.I. Philippopoulos. *Inorg. Chim. Acta*, **362**, 3079 (2009).
- [28] C.P. Matos, A. Valente, F. Marques, P. Adão, M.P. Paula Robalo, R.F.M. de Almeida, J.C. Pessoa, I. Santos, M.H. Helena Garcia, A.I. Tomaz. *Inorg. Chim. Acta*, **394**, 616 (2013).
- [29] M.M. Mohamed Subarkhan, R. Ramesh. *Spectrochim. Acta, Part A*, **138**, 264 (2015).
- [30] I.N. Booyesen, S. Maikoo, M.P. Akerman, B. Xulu. *Transition Met. Chem.*, **40**, 397 (2015).
- [31] J.H. Zagal, F. Bedioui, J.P. Dodelet (Eds). *N4-Macrocyclic Metal Complexes*, Springer, New York (2006).
- [32] P. Byabartta, S.K. Jasimuddin, G. Mostafa, T.-H. Lu, C. Sinha. *Polyhedron*, **22**, 849 (2003).
- [33] G. Zengin, C. Sarikurkcu, A. Aktumsek, R. Ceylan, O. Ceylan. *Ind. Crops Prod.*, **53**, 244 (2014).
- [34] P. Anitha, N. Chitrapriya, Y. Jang, P. Viswanathamurthi. *J. Photochem. Photobiol., B*, **129**, 17 (2013).
- [35] M.C.F. Simões, J.J.S. Sousa, A.A.C.C. Pais. *Cancer Lett.*, **357**, 8 (2015).
- [36] T.S. Sathiya Kamatchi, N. Chitrapriya, S.K. Kim, F.R. Fronczek, K. Natarajan. *Eur. J. Med. Chem.*, **59**, 253 (2013).
- [37] T.S. Kamatchi, N. Chitrapriya, V.S. Jamal Ahamed, S. Moon, F.R. Fronczek, K. Natarajan. *Inorg. Chim. Acta*, **404**, 58 (2013).
- [38] G. Prakash, R. Manikandan, P. Viswanathamurthi, K. Velmurugan, R. Nandhakumar. *J. Photochem. Photobiol., B*, **138**, 63 (2014).
- [39] J.P. da Silva, F.R. Caetano, D.A. Cavarzan, F.D. Fagundes, L.L. Romualdo, J. Ellena, M. Jaworska, P. Lodowski, A. Barison, M.P. de Araujo. *Inorg. Chim. Acta*, **373**, 8 (2011).
- [40] G. Tamasi, R. Cini. *J. Mol. Struct.*, **1048**, 27 (2013).
- [41] I. Turel, M. Pečanac, A. Golobič, E. Alessio, B. Serli, A. Bergamo, G. Sava. *J. Inorg. Biochem.*, **98**, 393 (2004).
- [42] A. Kanchanadevi, R. Ramesh, N. Bhuvanesh. *J. Organomet. Chem.*, **788**, 49 (2015).
- [43] K. Nagaraju, R. Raveendran, S. Pal, S. Pal. *Polyhedron*, **33**, 52 (2012).
- [44] G.D. Frey, Z.R. Bell, J.C. Jeffery, M.D. Ward. *Polyhedron*, **20**, 3231 (2001).
- [45] H. Brunner, T. Neuhierl, B. Nuber. *J. Organomet. Chem.*, **563**, 173 (1998).
- [46] H. Brunner, T. Neuhierl, B. Nuber. *Eur. J. Inorg. Chem.*, **1988**, 1877 (1988).
- [47] S.K. Patra, N. Sadhukhan, J.K. Bera. *Inorg. Chem.*, **45**, 4007 (2006).
- [48] H. Brunner, R. Oeschey, B. Nuber. *Organometallics*, **15**, 3616 (1996).